IEEE Access
Multidisciplinary | Rapid Review | Open Access Journal

Received August 20, 2021, accepted September 5, 2021, date of publication September 14, 2021,
date of current version September 27, 2021.

Digital Object Identifier 10.1109/ACCESS.2021.3112759

A Node-to-Node Admittance Functions Implementation of an Improved Frequency Dependent Multiconductor Transmission Line Model

YOUPENG HUANGFU, (Member, IEEE), LUCA DI RIENZO, (Senior Member, IEEE), AND SHULI YIN

Dipartimento di Elettronica, Informazione e Bioingegneria, Politecnico di Milano, 20133 Milan, Italy

Corresponding author: Shuli Yin (shuli.yin@polimi.it)

ABSTRACT The electromagnetic interference (EMI) performances of the interconnects and cables can be predicted via a standard multi-conductor transmission line (MTL) model, while the latter is not valid for the evaluation of power rail collapse and ground bounce responses. To circumvent the limitations, a more general and feasible improved MTL representation is presented in this paper. It physically incorporates the partial resistance and partial inductance parameters of all signal and reference conductors. To consider the frequency dependent behavior of the per-unit-length (PUL) electrical parameters in time domain simulations, a terminal description for this improved MTL model with any desired length is demonstrated. Subsequently, an equivalent node-to-node admittance functions (NAFs) implementation for this terminal representation is carried out. The correctness and effectiveness of the NAFs circuit model in time domain is then numerically validated by analyzing two dedicated examples.

INDEX TERMS Crosstalk, ground bounce, multi-conductor transmission line, time domain analysis.

I. INTRODUCTION

Electromagnetic compatibility (EMC) characteristics involved in electronic and electrical systems have been dramatically aggravated because of the increased operating frequency and decreased rising and falling times [1]–[6]. Generally, for the purpose of EMC predictions, the interconnects and cables in the systems can be analyzed by means of full-wave electromagnetic approaches [7]–[12], an electromagnetic topology principle [13]–[19], a Kron reduction technique [20]–[22], or a standard multi-conductor transmission line (MTL) model [23]–[27].

Specifically, the powerful standard MTL model is widely applied due to the simple implementation. Nevertheless, as can be noted, a subtle characteristic of this commonly used standard MTL model is that the general per-unit-length (PUL) loop electrical parameters, that is, loop resistances and loop inductances are adopted [24]. With this unique feature the wave equations for voltage and current signals can be analytically or numerically solved in time domain [28]–[37] or in frequency domain [38]–[47]. Alternatively, in frequency domain, the MTLs can be modeled via a macro-modeling approach based on this standard MTL representation [48].

As explained in [49]–[51], PUL loop resistances and loop inductances essentially involve the electrical properties both from the signal conductors and the reference one (or named ground). Typically, loop resistances and loop inductances can be placed in either the associated signal conductor or the reference one while they cannot be uniquely assigned to either conductor. Therefore, in the standard MTL model, the reference conductor is implicitly treated as an ideal one so that there is no longitudinal potential difference along it. As a consequence, the application of PUL loop resistance and loop inductance parameters makes the standard MTL model not applicable to predict the EMC phenomena related to the reference conductor. It means that the voltage drops across each conductor, such as the power rail collapse and ground bounce behaviors cannot be computed uniquely [51]. As a matter of fact, they are the primary cause of most EMI and must be evaluated correctly.

The associate editor coordinating the review of this manuscript and approving it for publication was Mohd Zainal Abidin Ab Kadir.

To cope with the issues raised above appropriately, the important concepts of partial resistances and partial inductances as opposed to loop resistances and loop inductances which are well discussed in [49]–[51] can be employed. In [35] and [36], an improved MTL model is presented and analyzed by introducing partial resistances and partial inductances. Nonetheless, the voltage across each conductor can not be uniquely computed. This is because in the finite difference time domain solution of the MTL equations the partial resistance and partial inductance parameters are transformed into the corresponding loop ones. As a result, only the loop voltages, that is, the voltages of signal conductors with respect to the reference one can be computed.

As it is well known, EMC predictions in time domain is intuitive, feasible, and highly desired since in this case both linear and nonlinear devices can be easily taken into consideration. Generally, in a wideband frequency range, interconnects and cables reveal to be frequency dependent coupled lossy MTLs. Losses of MTLs due to skin-, proximity-, and dispersive- effects can further adversely degrade the signal and power transmission quality [24]. As a matter of fact, the accurate and efficient representation of the frequency dependent parameters in time domain is very challenge while significant on the MTL modeling.

Therefore, in this paper, firstly an improved coupled lossy MTL representation is introduced. The PUL partial parameters, such as self- and mutual- partial resistances and partial inductances for all conductors including reference ones are considered. A terminal description of the improved MTL representation with a desired length is then presented. Next, to involve frequency dependent PUL parameters in time domain, the broadband terminal admittance matrix (TAM) representation for this terminal description model of an MTLs is numerically extracted via a frequency sweep analysis. A passive reduced order model for the TAM is then achieved via a matrix rational approximations (MRAs) technique. Finally, a node-to-node admittance functions (NAFs) implementation for the rational model of the terminal description representation can be applied.

For the numerical validation work in time domain, two dedicated test cases are analyzed in terms of the voltage responses, such as ground bounce, power rail collapse, and crosstalk. The time domain results are verified against a reference Inverse Fast Fourier Transform (IFFT) approach.

II. DESCRIPTION OF THE IMPROVED MTL REPRESENTATION

A. IMPROVED MTL REPRESENTATION

Firstly, let us consider a coupled homogeneous $(M+1)$-conductor $(M \geq 1)$ MTLs with any desired length. It is sketched in FIGURE 1. As can be noted, the reference conductor (labeled #0) is regarded as a non-ideal one. Observe that as an equivalent, the MTLs with the desired length can be represented by an interface terminal description with in total $(2M+2)$-terminal (both ends of the $(M+1)$-conductor). Note that the left and right terminals of the reference conductor

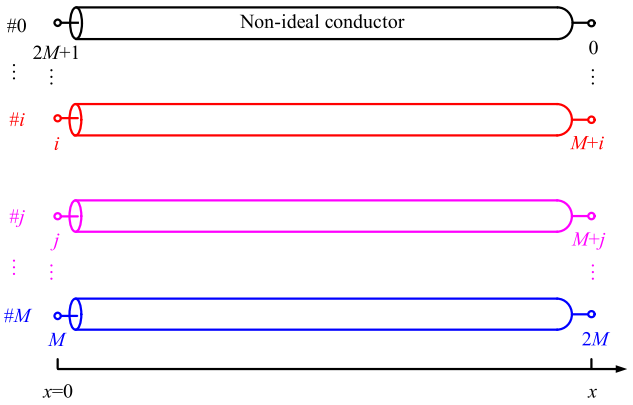

FIGURE 1. A terminal description for a uniform $(M+1)$-conductor MTLs with any desired length.

are numbered as $(2M+1)$ and 0, respectively. Therein, terminal 0 is identified as the voltage reference for all the other terminals and its choice can be somehow arbitrary.

In a given frequency range, let us consider an electrically small section (Δx) of an MTLs under the quasi transverse electromagnetic (TEM) approximation. This PUL section can be equivalent to an improved distributed parameter MTL representation (FIGURE 2) by incorporating partial resistances and partial inductances [49]–[51]. As illustrated in FIGURE 2, the partial inductances and partial resistances are uniquely ascribed to each conductor; r_{pii} and l_{pii} $(i = 0, 1, \ldots, M)$ represent the PUL self partial resistances and self partial inductances for each conductor, respectively; r_{pij} and l_{pij} $(i, j = 0, 1, \ldots, M)$ are the PUL mutual partial resistances and mutual partial inductances between conductors i and j, respectively. Note that elements g_{ij} and c_{ij} $(i, j = 1, 2, \ldots, M)$ indicate the PUL conductance and capacitance parameters, respectively.

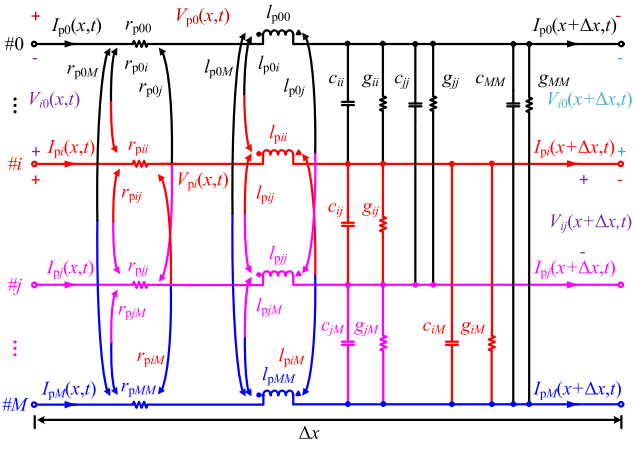

FIGURE 2. An improved MTL representation of an electrically small section Δx for an $(M+1)$-conductor MTLs in time domain.

B. UNDERSTANDING OF POWER RAIL COLLAPSE AND GROUND BOUNCE

With reference to FIGURE 2, the partial voltage drops $V_{pi}(x,t)$ across each signal conductor i ($i = 1, 2, \ldots, M$) and $V_{p0}(x,t)$ across the reference one are typically defined as power rail collapse and ground bounce responses, respectively [50], [51]. They can be physically written in a concise matrix form:

$$\mathbf{V}_{\mathrm{p}}(x,t) = \mathbf{R}_{\mathrm{p}}\Delta x \mathbf{I}_{\mathrm{p}}(x,t) + \mathbf{L}_{\mathrm{p}}\Delta x \frac{\partial \mathbf{I}_{\mathrm{p}}(x,t)}{\partial t} \tag{1}$$

where

$$\mathbf{V}_{\mathrm{p}}(x,t) = \begin{bmatrix} V_{\mathrm{p}0}(x,t) \\ V_{\mathrm{p}1}(x,t) \\ \vdots \\ V_{\mathrm{p}i}(x,t) \\ \vdots \\ V_{\mathrm{p}M}(x,t) \end{bmatrix} \tag{2}$$

and

$$\mathbf{I}_{\mathrm{p}}(x,t) = \begin{bmatrix} I_{\mathrm{p}0}(x,t) \\ I_{\mathrm{p}1}(x,t) \\ \vdots \\ I_{\mathrm{p}i}(x,t) \\ \vdots \\ I_{\mathrm{p}M}(x,t) \end{bmatrix} \tag{3}$$

are $(M+1)\times 1$ partial voltage and current vectors, respectively; in addition

$$\mathbf{R}_{\mathrm{p}} = \begin{bmatrix} r_{\mathrm{p}00} & r_{\mathrm{p}01} & \cdots & r_{\mathrm{p}0i} & \cdots & r_{\mathrm{p}0M} \\ r_{\mathrm{p}10} & r_{\mathrm{p}11} & \cdots & r_{\mathrm{p}1i} & \cdots & r_{\mathrm{p}1M} \\ \vdots & \vdots & \ddots & \vdots & \ddots & \vdots \\ r_{\mathrm{p}i0} & r_{\mathrm{p}i1} & \cdots & r_{\mathrm{p}ii} & \cdots & r_{\mathrm{p}iM} \\ \vdots & \vdots & \ddots & \vdots & \ddots & \vdots \\ r_{\mathrm{p}M0} & r_{\mathrm{p}M1} & \cdots & r_{\mathrm{p}Mi} & \cdots & r_{\mathrm{p}MM} \end{bmatrix} \tag{4}$$

and

$$\mathbf{L}_{\mathrm{p}} = \begin{bmatrix} l_{\mathrm{p}00} & l_{\mathrm{p}01} & \cdots & l_{\mathrm{p}0i} & \cdots & l_{\mathrm{p}0M} \\ l_{\mathrm{p}10} & l_{\mathrm{p}11} & \cdots & l_{\mathrm{p}1i} & \cdots & l_{\mathrm{p}1M} \\ \vdots & \vdots & \ddots & \vdots & \ddots & \vdots \\ l_{\mathrm{p}i0} & l_{\mathrm{p}i1} & \cdots & l_{\mathrm{p}ii} & \cdots & l_{\mathrm{p}iM} \\ \vdots & \vdots & \ddots & \vdots & \ddots & \vdots \\ l_{\mathrm{p}M0} & l_{\mathrm{p}M1} & \cdots & l_{\mathrm{p}Mi} & \cdots & l_{\mathrm{p}MM} \end{bmatrix} \tag{5}$$

are $(M+1)\times(M+1)$ PUL partial resistance and partial inductance matrices, respectively.

The quasi-TEM assumption implies the current relations

$$I_{\mathrm{p}0}(x,t) = -\sum_{i=1}^{M} I_{\mathrm{p}i}(x,t) \tag{6}$$

where $I_{\mathrm{p}0}(x,t)$ and $I_{\mathrm{p}i}(x,t)$ ($i = 1, 2, \ldots, M$) are governed respectively by

$$\begin{aligned} I_{\mathrm{p}0}(x,t) = {} & c_{11}\frac{\partial V_{01}(x+\Delta x,t)}{\partial t} + g_{11}V_{01}(x+\Delta x,t) \\ & + \cdots + c_{ii}\frac{\partial V_{0i}(x+\Delta x,t)}{\partial t} + g_{ii}V_{0i}(x+\Delta x,t) \\ & + \cdots + c_{MM}\frac{\partial V_{0M}(x+\Delta x,t)}{\partial t} \\ & + g_{MM}V_{0M}(x+\Delta x,t) + I_{\mathrm{p}0}(x+\Delta x,t) \end{aligned} \tag{7}$$

and

$$\begin{aligned} I_{\mathrm{p}i}(x,t) = {} & c_{i1}\frac{\partial V_{i1}(x+\Delta x,t)}{\partial t} + g_{i1}V_{i1}(x+\Delta x,t) \\ & + \cdots + c_{ii}\frac{\partial V_{i0}(x+\Delta x,t)}{\partial t} + g_{ii}V_{i0}(x+\Delta x,t) \\ & + \cdots + c_{iM}\frac{\partial V_{iM}(x+\Delta x,t)}{\partial t} \\ & + g_{iM}V_{iM}(x+\Delta x,t) + I_{\mathrm{p}i}(x+\Delta x,t) \end{aligned} \tag{8}$$

where $V_{ij}(x+\Delta x,t)$ is the voltage across the terminals i and j.

It can be noted that from (1) the partial voltage vector $\mathbf{V}_{\mathrm{p}}(x,t)$ across each conductor depends on the self- and mutual- partial resistances and inductances and current vector $\mathbf{I}_{\mathrm{p}}(x,t)$. As shown in (7) and (8) the partial currents are associated with mutual capacitances and conductances and also with the voltage across each two terminals.

A remark is due here. For the case of frequency independent PUL parameters, (2) and (3) in time domain can be numerically obtained by simulating enough cascaded electrically small sections. On the contrary, for the case of frequency dependent PUL parameters, the time domain responses of an MTLs can be obtained by using the IFFT approach [52]. Although it is only applicable for linear terminations and can be time consuming for a wide frequency band and a long MTLs, it provides a reference solution for the validation purposes in this paper. In Section III, an alternative yet more efficient time domain approach is presented for an MTLs with frequency dependent PUL parameters based on the terminal description.

III. NAFs IMPLEMENTATION FOR THE IMPROVED MTL MODEL WITH FREQUENCY DEPENDENT PARAMETERS

A. TAM REPRESENTATION OF THE IMPROVED MTL MODEL WITH A DESIRED LENGTH

Consider an MTLs with the desired length based on an elementary section of improved MTL model in FIGURE 2. Following [53] the $(2M+2)$-terminal description (FIGURE 1) of the improved MTL model can be represented by an NAFs circuit network $\mathbf{y}(s)$ (s is the Laplace variable) totally including $(M+1)\times(2M+1)$ equivalent admittance elements. This model is illustrated in FIGURE 3 in detail. It can be noted that, each pair of terminals is associated with an admittance element: element $y_{i,i}(s)$ ($i = 1, 2, \ldots, 2M+1$) is the self-admittance between terminal i and the reference 0; while element $y_{i,j}(s)$ ($i, j = 1, 2, \ldots, 2M+1$, and $i \neq j$) indicates the mutual-admittance between terminals i and j.

Referring to FIGURE 3, assume that terminal i ($i = 1, 2, \ldots, 2M+1$) is excited by a sinusoidal voltage source u_i with respect to the voltage reference terminal 0. Then the current i_i flowing into the terminal i can be given by:

$$i_i = i_{i,\,1} + \cdots + i_{i,\,i} + \cdots + i_{i,\,2M+1} \tag{9}$$

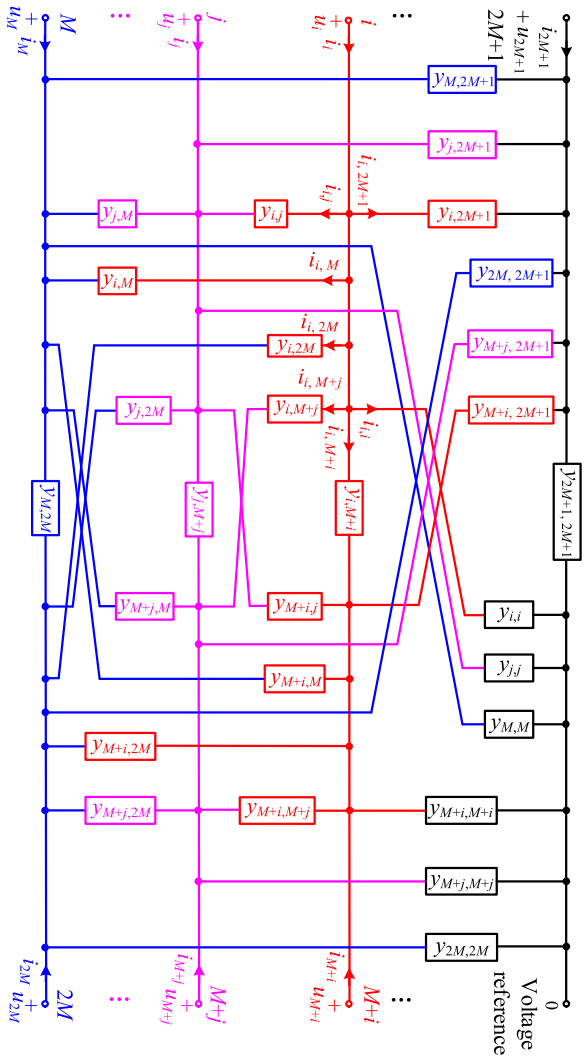

FIGURE 3. An equivalent NAFs network of an improved MTL model with the desired length.

where branch currents $i_{i,j}$ ($i, j = 1, 2, \ldots, 2M+1$) and voltages u_i associated with terminal i are linked via admittances $y_{i,j}$:

$$\begin{cases} i_{i,\,1} = y_{i,\,1}\,(u_i - u_1) \\ \vdots \\ i_{i,\,i} = y_{i,\,i} u_i \\ \vdots \\ i_{i,\,2M+1} = y_{i,\,2M+1}\,(u_i - u_{2M+1}) \end{cases} \tag{10}$$

Substituting (10) into (9) yields:

$$\begin{aligned} i_i = {} & \left(y_{i,\,1} + \cdots + y_{i,\,i} + \cdots + y_{i,\,M} + y_{i,\,M+1}\right. \\ & \left. + \cdots + y_{i,\,2M+1}\right) u_i \\ & - \left(y_{i,\,1} u_1 + \cdots + y_{i,\,i-1} u_{i-1} + y_{i,\,i+1} u_{i+1}\right. \\ & \left. + \cdots + y_{i,\,2M+1} u_{2M+1}\right) \end{aligned} \tag{11}$$

or, in a compact matrix form for all terminals, one obtains:

$$\mathbf{i}\,(s)_{(2M+1)\times 1} = \mathbf{Y}\,(s)_{(2M+1)\times(2M+1)}\,\mathbf{u}\,(s)_{(2M+1)\times 1} \tag{12}$$

where $\mathbf{i}(s)$ is terminal current vector and $\mathbf{u}(s)$ is the terminal voltage vector with respect to reference 0; and they are:

$$\begin{cases} \mathbf{i}\,(s)_{(2M+1)\times 1} = [i_1,\ \cdots, i_i,\ \cdots,\ i_{2M+1}]^{\mathrm{T}} \\ \mathbf{u}\,(s)_{(2M+1)\times 1} = [u_1,\ \cdots, u_i,\ \cdots,\ u_{2M+1}]^{\mathrm{T}} \end{cases} \tag{13}$$

In (12), the symmetric $\mathbf{Y}(s)$ represents the TAM of the improved MTL model with any desired length. It reads

$$\mathbf{Y}\,(s) = \begin{bmatrix} Y_{1,1}\,(s) & \cdots & Y_{1,i}\,(s) & \cdots & Y_{1,2M+1}\,(s) \\ \vdots & \ddots & \vdots & \ddots & \vdots \\ Y_{i,1}\,(s) & \cdots & Y_{i,i}\,(s) & \cdots & Y_{i,2M+1}\,(s) \\ \vdots & \ddots & \vdots & \ddots & \vdots \\ Y_{2M+1,1}\,(s) & \cdots & Y_{2M+1,i}\,(s) & \cdots & Y_{2M+1,2M+1}\,(s) \end{bmatrix} \tag{14}$$

with matrix elements defined as

$$Y_{i,i}\,(s) = \sum_{j=1}^{2M+1} y_{i,j}\,(s) \tag{15}$$

and

$$Y_{i,j}\,(s) = -y_{i,j}\,(s) \tag{16}$$

for $i \neq j$.

Substituting (16) into (15) yields

$$y_{i,i}\,(s) = \sum_{j=1}^{2M+1} Y_{i,j}\,(s) \tag{17}$$

so that (16) can be rewritten as

$$y_{i,j}\,(s) = -Y_{i,j}\,(s) \tag{18}$$

for $i \neq j$.

Remark that in this paper, the entries $Y_{i,j}(s)$ of TAM are defined with uppercase letters while the circuit elements $y_{i,j}(s)$ are defined with lowercase ones.

B. EXTRACTION OF TAM

In this sub-section, two different approaches, that is an indirect method and a direct method are presented in order to numerically extract the TAM $\mathbf{Y}(s)$ in (14) for an MTLs. Basically, the improved MTL model in Laplace domain depicted in FIGURE 4 is adopted for the two approaches. Note that enough cascaded sections must be employed to achieve the desired length of an MTLs for the frequency sweep analysis in the prescribed frequency samples.

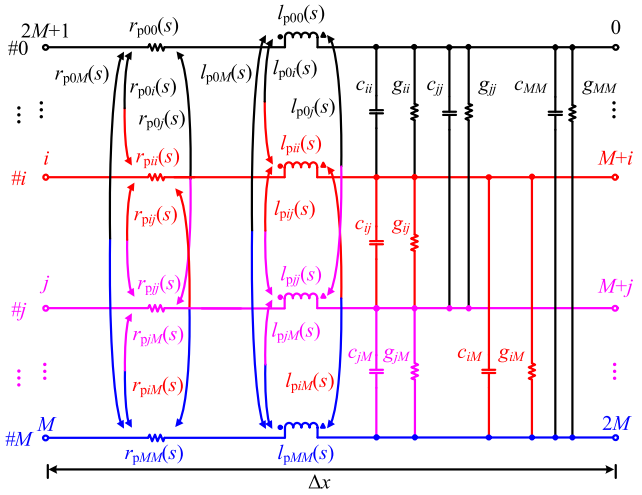

FIGURE 4. Laplace domain representation of the improved MTL model for an elementary section.

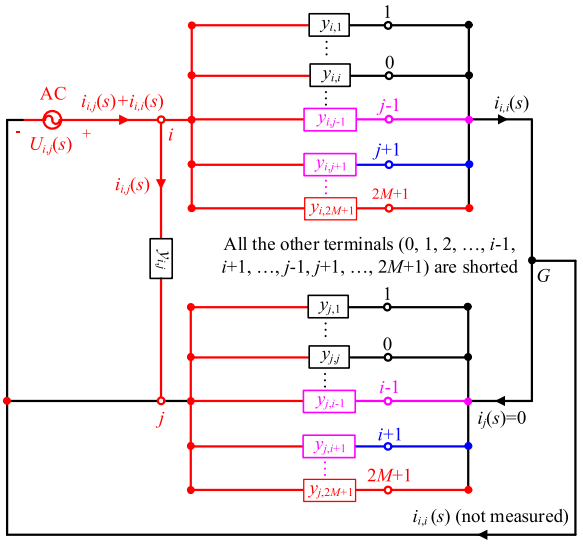

FIGURE 5. Extraction schematic of $y_{i,j}(s)$ for an MTLs with desired length.

In FIGURE 4, the frequency dependent PUL partial resistance and inductance parameters can be numerically evaluated by using a quasi-static magnetic field solver, e.g. [54]. Observe that the frequency dependent behaviors of the capacitances and the conductances are neglected. They can be computed via the static electric field solver [54].

1) INDIRECT METHOD

The indirect extraction of TAM means that the admittance elements $y_{i,j}(s)$ $(i, j = 1, 2, \ldots, 2M + 1)$ will be evaluated prior to $\mathbf{Y}(s)$.

Based on the improved MTL model in FIGURE 4, $y_{i,j}(s)$ $(i, j = 1, 2, \ldots, 2M + 1)$ of an MTLs with desired length can be computed by using an AC analysis method with the aid of circuit simulators. In this paper, the MATLAB/Simulink platform is preferred since the circuit model in Simulink can be easily invoked through a script in MATLAB.

The evaluation schematic of $y_{i,j}(s)$ for the indirect approach is illustrated in FIGURE 5 [55]. The procedures can be organized as follows: (1) in the frequency range of interest, determine the total sections of an MTLs to achieve the given length. (2) As depicted, apply an AC voltage source $U_{i,j}(s)$ with unit amplitude between terminals i and j. (3) Short all remaining terminals, and then connect this new point of presence G to the negative terminal of the source supply. In this case terminals G and j share the same electric potential. This means that $i_j(s) = 0$. (4) Perform a frequency sweep analysis in the frequency range of interest in order to collect the targeted current $i_{i,j}(s)$. Finally, $y_{i,j}(s)$ can be evaluated as

$$y_{i,j}(s) = \frac{i_{i,j}(s)}{U_{i,j}(s)} \tag{19}$$

Subsequently, all other admittance elements associated with NAFs $\mathbf{y}(s)$ can be obtained by using this well-defined procedure. Therefore, one can easily obtain the desired $\mathbf{Y}(s)$ via (15) and (16). However, a remarkable drawback of this indirect method is that $(M + 1)\times(2M + 1)/2$ times simulations must be carried out considering the symmetric property of $\mathbf{y}(s)$.

2) DIRECT METHOD

Alternatively, a direct approach is introduced in this subsection. It is a preferred and more efficient numerical method compared with the indirect one. In this approach, the numerical simulation setup for evaluating TAM $\mathbf{Y}(s)$ for an MTLs with the desired length can be represented in FIGURE 6 (a). Therein, terminal i $(i = 1, 2, \ldots, 2M + 1)$ is activated by an AC voltage source $U_i(s)$ while the others are short-circuited to the reference terminal 0.

The equivalent circuit of FIGURE 6 (a) can be detailly represented in FIGURE 6 (b). Due to the short-circuit connections, only circuit elements $y_{i,j}(s)$ $(j = 1, 2, \ldots, 2M + 1)$ remain. According to the Kirchhoff's current law and in terms of terminal i, one obtains:

$$I_i(s) = -\left[I_{i,1}(s) + \cdots + I_{i,i}(s) + \cdots + I_{i,2M+1}(s)\right] \tag{20}$$

In FIGURE 6 (b), the relationship between $I_{i,j}(s)$ and voltage source $U_i(s)$ is given by

$$\begin{cases} I_{i,1}(s) = -y_{i,1}(s)\, U_i(s) \\ \vdots \\ I_{i,i}(s) = -y_{i,i}(s)\, U_i(s) \\ \vdots \\ I_{i,2M+1}(s) = -y_{i,2M+1}(s)\, U_i(s) \end{cases} \tag{21}$$

Substituting (15) and (21) into (20) yields:

$$I_i(s) = \sum_{j=1}^{2M+1} y_{i,j}(s)\, U_i(s) = Y_{i,i}(s)\, U_i(s) \tag{22}$$

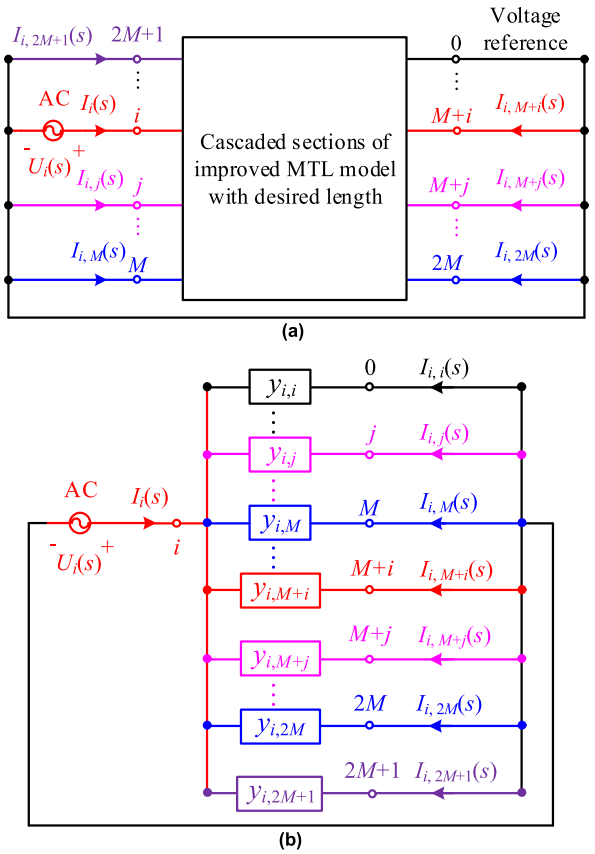

FIGURE 6. Direct extraction of TAM for an MTLs with desired length: (a) numerical simulation setup, and (b) its equivalent circuit representation.

Substituting (16) into (21) yields:

$$\begin{cases} I_{i,\,1}\,(s) = Y_{i,\,1}\,(s)\,U_i\,(s) \\ \vdots \\ I_{i,\,i-1}\,(s) = Y_{i,\,i-1}\,(s)\,U_i\,(s) \\ I_{i,\,i+1}\,(s) = Y_{i,\,i+1}\,(s)\,U_i\,(s) \\ \vdots \\ I_{i,2M}\,(s) = Y_{i,2M}\,(s)\,U_i\,(s) \end{cases} \tag{23}$$

Combining (22) and (23), the i-th row entry $Y_{i,j}(s)$ ($j = 1, 2, \ldots, 2M+1$) can be obtained by evaluating $I_{i,j}(s)$, so that

$$Y_{i,j}(s) = \frac{I_{i,\,j}(s)}{U_i(s)} \tag{24}$$

Remark that with this direct approach, one can easily achieve a row of $\mathbf{Y}(s)$ with only once frequency sweep computation. As a result, $(M+1)$ circuit simulations in total are required for an $(M+1)$-conductor MTLs. Clearly the direct approach for evaluating $\mathbf{Y}(s)$ is more computationally efficient compared to the indirect one.

Obviously, from (17) and (18), if $Y_{i,j}(s)$ can be rationally approximated, as a consequence $y_{i,j}(s)$ will be automatically achieved also in a rational representation. Note that the two rational models share the same set of poles. The following sub-section introduces a methodology that represents $\mathbf{Y}(s)$ with a stable and passive rational approximation. Then a circuit synthesis method of rational model of $\mathbf{y}(s)$ is given.

C. MRAs FOR TAM

With a straightforward rational approximation by using the MRAs approach [56]–[58] and a passivity enforcement method [59]–[60], the obtained TAM $\mathbf{Y}(s)$ for an improved MTL model with the desired length can be expressed by a passive partial fraction expansion:

$$\mathbf{Y}\,(s) \approx \mathbf{Y}_{\rm rat}\,(s) = \sum_{n=1}^{N} \frac{\mathbf{C}_n}{s - \boldsymbol{a}_n} + \mathbf{D} + s\mathbf{H} \tag{25}$$

which satisfies the following passivity requirements

$$\begin{cases} \text{eig}\,(\text{Re}\,\{\mathbf{Y}_{rat}(s)\}) > 0 \\ \text{eig}\,(\mathbf{D}) > 0 \\ \text{eig}\,(\mathbf{H}) > 0 \end{cases} \tag{26}$$

where N is the degree of the approximation; $\boldsymbol{a}$ and $\mathbf{C}$ are the vector of the common poles and the matrix of the residues, respectively; $\mathbf{D}$ and $\mathbf{H}$ are the matrices of constant and proportional terms, respectively. Specifically, "eig" denotes evaluation of eigenvalues. The numerical implementation of (26) can be achieved by perturbation of the eigenvalues of these matrices with minimal changes [59]–[60].

From (25), using (17)-(18) one obtains

$$y_{i,i}\,(s) = \sum_{n=1}^{N} \frac{\boldsymbol{k}_n}{s - \boldsymbol{a}_n} + p + sq \tag{27}$$

with

$$\begin{cases} \boldsymbol{k}_n = \sum\limits_{j=1}^{2M+1} \left(\mathbf{C}_{ij}\right)_n \\ p = \sum\limits_{j=1}^{2M+1} \mathbf{D}_{ij} \\ q = \sum\limits_{j=1}^{2M+1} \mathbf{H}_{ij} \end{cases} \tag{28}$$

and

$$y_{i,j}\,(s) = \sum_{n=1}^{N} \frac{\boldsymbol{u}_n}{s - \boldsymbol{a}_n} + v + sw \tag{29}$$

for $i \neq j$ and in which

$$\begin{cases} \boldsymbol{u}_n = -\left(\mathbf{C}_{ij}\right)_n \\ v = -\mathbf{D}_{ij} \\ w = -\mathbf{H}_{ij} \end{cases} \tag{30}$$

To this extent, the rational approximation representations of NAFs $\mathbf{y}(s)$ are obtained based on the admittances defined by (27) and (29).

Then following the circuit synthesis approach in [61] the frequency dependent rational representations in (27) and (29), that is, constant terms and s-proportional terms, real pole terms, and complex pole terms can be synthesized as equivalent circuits that only with constant circuit elements.

Eventually, the NAFs circuit model for the improved MTL representation with the desired length can be realized.

IV. NUMERICAL VALIDATIONS

Practical applications of the presented NAFs circuit model based on the improved MTL representation are illustrated in this section. Two numerical examples for the analysis of power rail collapse, ground bounce, and crosstalk voltage responses are carried out. The well-known IFFT approach [52] is performed for the numerical validation purpose.

A. A TWO-CONDUCTOR DIGITAL MTLs SYSTEM

As a first example, consider a typical two-conductor digital MTLs. It is interfaced with transmitter and receiver drivers, as illustrated in FIGURE 7 (a). The interconnects include 2 coupled parallel circular power pins (S1 and S2) and a shared ground pin (G). The pin pattern and its geometrical dimensions are described in FIGURE 7 (b).

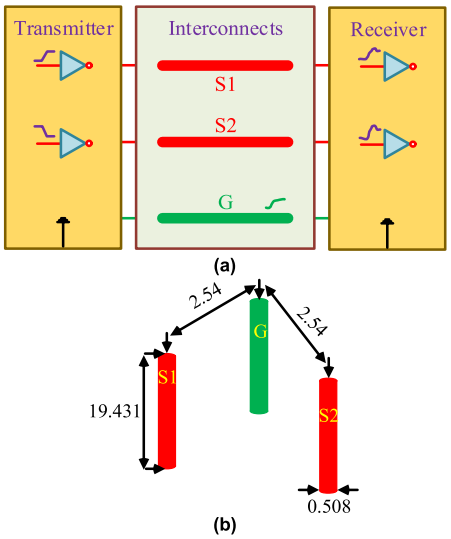

FIGURE 7. (a) A typical two-conductor digital MTLs system interfaced with transmitter and receiver drivers; and (b) pin pattern with 2 power pins (in red) and 1 shared ground pin (in green); units are [mm].

For simplicity, suppose the excitation voltage source of this MTLs is characterized by a trapezoidal pulse (FIGURE 8 (a)) with $A = 5$, $t_{on} = 50$ ns, and $T = 100$ ns. In this test, two values for rising and falling times $t_r = t_f = 100$ ps and $t_r = t_f = 200$ ps are considered to investigate the influence on transient responses. Simplifying the MTLs system with resistive source loads at the near end (NE) and frequency dependent capacitive loads at the far end (FE) leads to an equivalent circuit representation as in FIGURE 8 (b).

The bandwidth concerned herein is from 10 MHz to 10 GHz with a uniform step of 10 MHz. To extract the TAM accurately and efficiently, 10 cascaded PUL sections and the direct method are employed. Then, a 12th-order rational model (6 real poles and 3 complex conjugate pole pairs) in (25) is applied to achieve a good approximation for TAM.

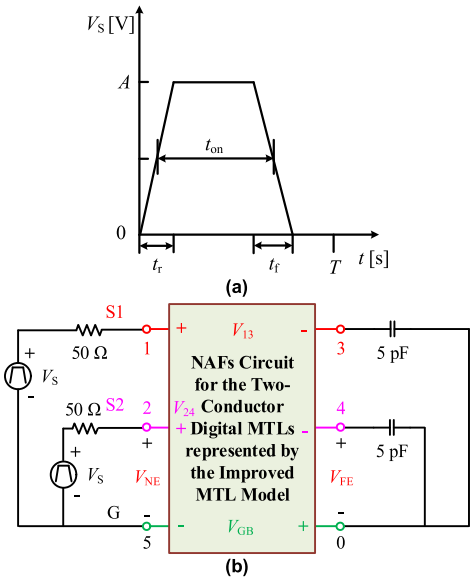

FIGURE 8. (a) Trapezoidal voltage excitation, and (b) circuit schematic representation of the digital MTLs system with capacitive loads.

In this paper, a PC with an Inter(R) Core(TM) i7 CPU at 3.07 GHz with 12 GB of memory is employed. For this test, the computational times of the NAFs model and the IFFT approach with the same time step of 1 ps are reported in TABLE 1. This confirms that the NAFs model is more computationally efficient than the reference IFFT solution.

TABLE 1. Computational times using NAFs model and IFFT method.

Model	NAFs	IFFT
Computational time	18.72 s	20.05 min

The ground bounce voltage responses (V_{GB}) obtained by using different rising times and excitation source patterns are presented in FIGURE 9. Therein, "S1" indicates that only signal conductor 1 is excited, while "S1S2" implies that conductors 1 and 2 are activated simultaneously.

The power rail collapse voltage responses V_{13} and V_{24} are reproduced in FIGURE 10 (a) and (b), respectively. In addition, the NE and FE crosstalk responses V_{NE} and V_{FE} are presented in FIGURE 11 (a) and (b), respectively. Note that only signal conductor 1 is activated ("S1") in this case.

From FIGURE 9, FIGURE 10, and FIGURE 11, a general conclusion can be drawn that using a smaller rising time (100 ps) can further degrade the EMC performances, since the ground bounce, power rail collapse, and crosstalk responses are increased accordingly. Additionally, from FIGURE 9, the same conclusion holds when more signal conductors are activated ("S1S2") simultaneously. The oscillations in the voltage responses implies that the MTLs cannot transmit the signals with sufficient fidelity.

To characterize the accuracy of the proposed NAFs model, a root-mean-square (RMS) error is adopted. It can be

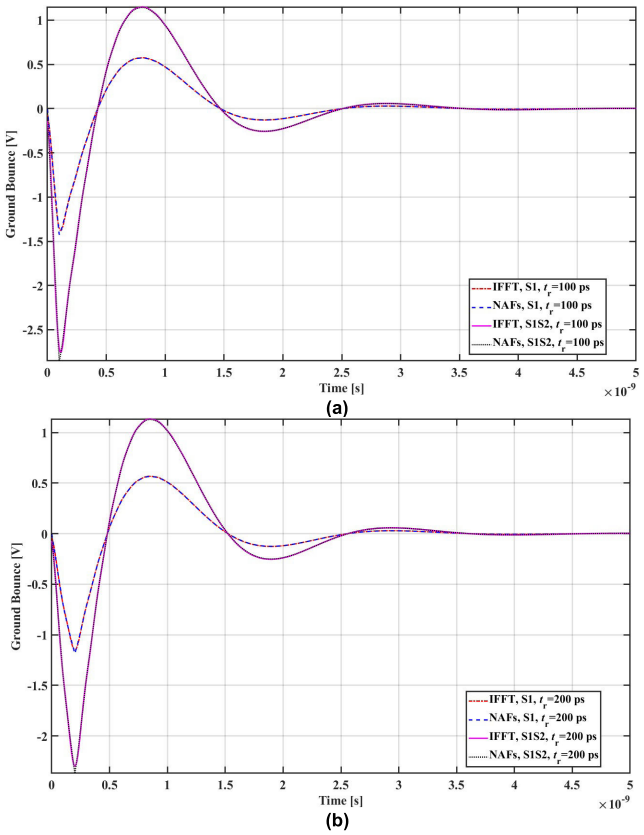

FIGURE 9. Ground bounce responses V_{GB} with different rising times and source excitation patterns: (a) $t_r = 100$ ps, and (b) $t_r = 200$ ps.

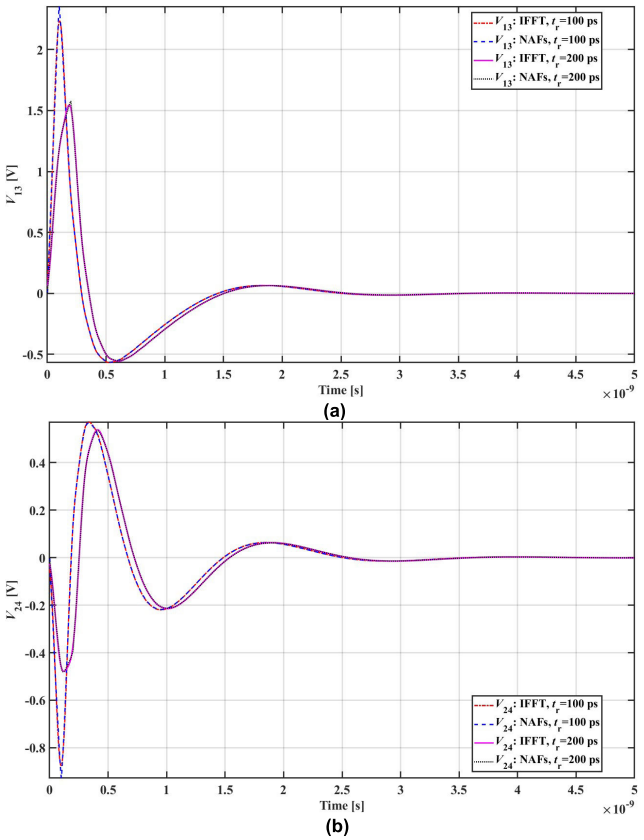

FIGURE 10. Power rail collapse voltage responses by using different rising times and by activating conductor 1 ("S1"): (a) V_{13}, and (b) V_{24}.

mathematically defined by

$$V_{\text{RMS error}} = \sqrt{\frac{\sum_{n=1}^{N_s} \left(V_n^{\text{IFFT}} - V_n^{\text{NAFs}}\right)^2}{N_s}} \tag{31}$$

where $V_{\text{RMS error}}$ is the RMS error for the concerned voltage response; N_s is the total time instants; V_n^{IFFT} and V_n^{NAFs} are the voltage responses computed via reference IFFT technique and NAFs model, respectively.

In this test case, the RMS errors for voltage responses V_{GB}, V_{13}, V_{24}, V_{NE}, and V_{FE} are reported in TABLE 2. Obviously, for all the concerned voltage responses, good agreements with respect to the results obtained from the IFFT solution are achieved.

B. A FOUR-CONDUCTOR SHIELDED POWER CABLE

In this test, a four-conductor shielded power cable for low voltage applications is considered. Its geometric description and dimensions are illustrated in FIGURE 12 and TABLE 3. The three-phase conductors U, V, and W, the ground conductor G, and the shield S are considered for the cable modeling. The frequency range from 100 kHz to 100 MHz with 1000 linearly spaced frequency samples is concerned. A cable sample of 1 m is investigated. 10 electrically small sections are cascaded to acquire the TAM. Then an 18th-order rational model in (25) is applied in order to achieve a good approximation for the TAM of the power cable.

The time domain simulation setup for the validation of the proposed NAFs model is illustrated in FIGURE 13. Again, a trapezoidal voltage source in FIGURE 8 (a) is used, where $A = 1$, $T = 10$ µs, $t_{\text{on}} = 900$ ns, and $t_{\text{r}} = t_{\text{f}} = 10$ ns.

TABLE 2. RMS errors for the digital MTLs.

t_{r}	Source Pattern	Voltage Response		RMS Error
100 ps	S1	Ground bounce	V_{GB}	0.55%
	S1S2			1.09%
	S1	Power rail collapse	V_{13}	1.00%
	S1		V_{24}	0.48%
	S1	Crosstalk	V_{NE}	0.34%
	S1		V_{FE}	0.29%
200 ps	S1	Ground bounce	V_{GB}	0.30%
	S1S2			0.60%
	S1	Power rail collapse	V_{13}	0.52%
	S1		V_{24}	0.26%
	S1	Crosstalk	V_{NE}	0.32%
	S1		V_{FE}	0.30%

TABLE 3. Dimensions of the power cable ([mm]).

Item	r_1	r_2	d_1	d_2	d_3	d_4	d_5
Value	1.382	0.691	19.5	3.92	3.66	3.46	4.6
Item	d_6	d_7	d_8	d_9	d_{10}	d_{11}	d_{12}
Value	1.60	4.60	8.00	9.23	4.56	1.58	1.58

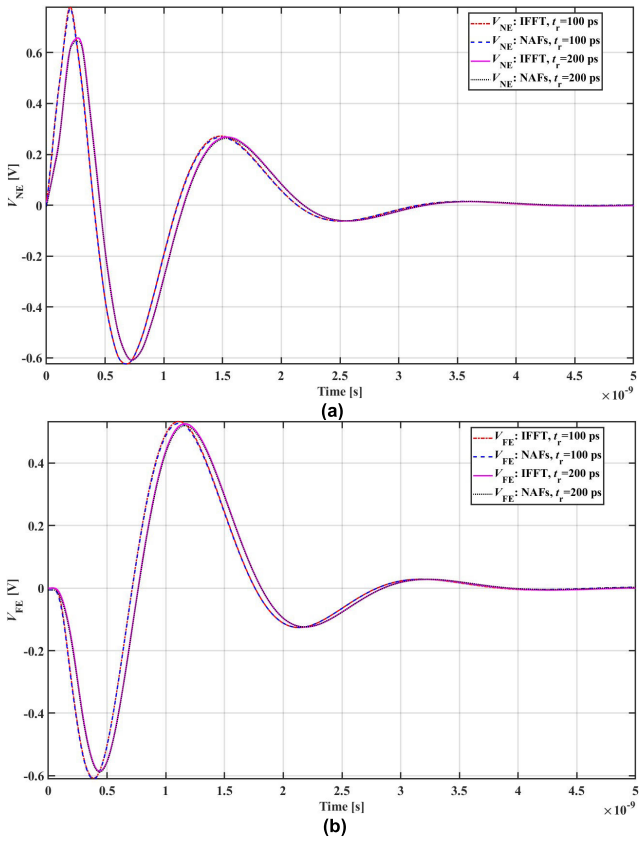

FIGURE 11. Crosstalk responses by using different rising times and by activating conductor 1 ("S1"): (a) V_{NE}, and (b) V_{FE}.

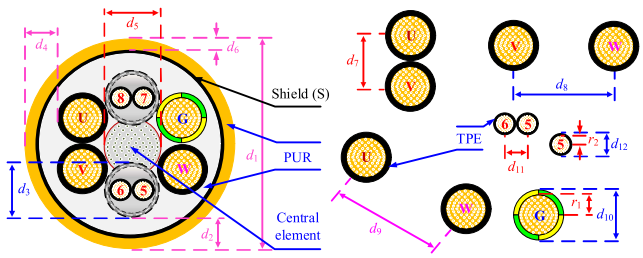

FIGURE 12. Geometric description of the four-conductor shielded cable.

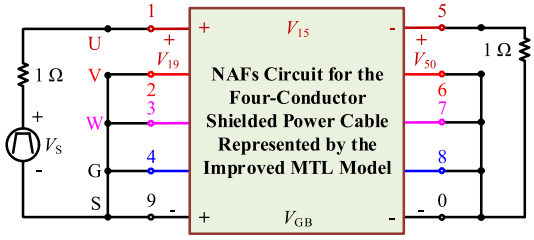

FIGURE 13. Time domain simulation setup of the power cable.

The computational times of the NAFs circuit and the reference IFFT solution by using the same time step of 1 ns are reported in TABLE 4. This clearly shows the high computational efficiency of the presented NAFs model.

TABLE 4. Computational times using NAFs model and IFFT method.

Model	NAFs	IFFT
Computational time	54.86 s	83.04 min

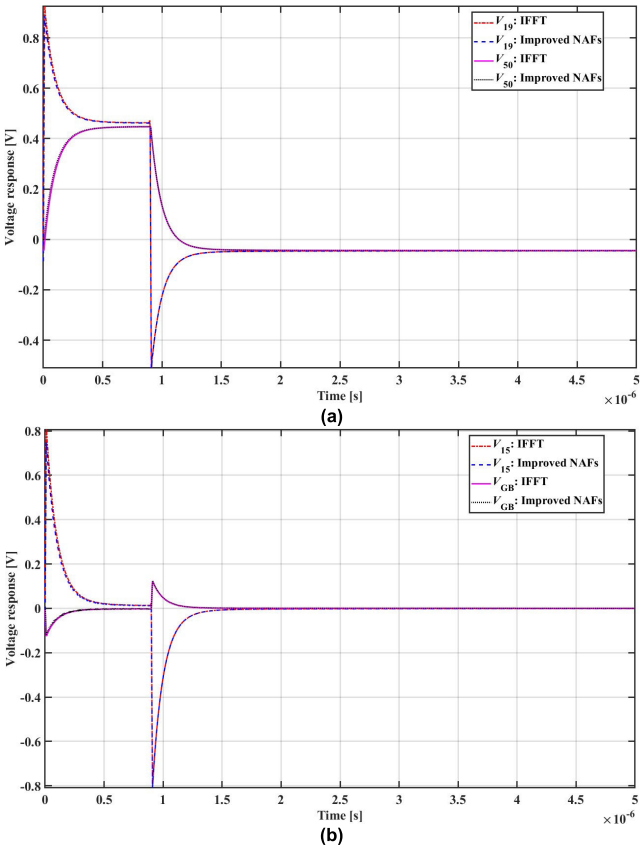

FIGURE 14. Voltage responses obtained from NAFs model, compared with the IFFT solution: (a) V_{19} and V_{50}, and (b) V_{15} and V_{GB}.

TABLE 5. RMS errors for the shielded power cable.

Voltage Response	RMS Error
V_{19}	0.48%
V_{50}	0.43%
V_{15}	0.77%
V_{GB}	0.15%

The voltage responses V_{19}, V_{50}, V_{15}, and V_{GB} defined in FIGURE 13 are shown in FIGURE 14 (a) and (b). The corresponding RMS errors are reported in TABLE 5. It can be noted that very accurate results are obtained compared with the reference IFFT solution, confirming the effectiveness and accuracy of the presented model.

V. CONCLUSION

In this paper, an improved MTL representation based on the introduction of the PUL partial resistance and partial inductance parameters is presented. It circumvents the limitations of the standard MTL representation and enables the

unique computation of power rail collapse and ground bounce responses. Then the terminal description of the improved MTL representation with a desired length is demonstrated. In time domain, to consider the frequency dependent PUL parameters, an NAFs circuit model is implemented for the terminal description of improved MTL model with the aid of matrix rational approximations and circuit synthesis technique. Time domain voltage responses obtained from the NAFs model indicate a high computational accuracy against to the reference IFFT solution and confirm a computational effort reduction. The implemented model can be extended to nonuniform and more complex MTLs with any desired length and geometry. By utilizing this model, EMC issues, especially the responses of ground bounce and power rail collapse, raised by interconnects and cables can be addressed and further minimized efficiently.

REFERENCES

[1] *Adjustable Speed Electrical Power Drive Systems—Part 3: EMC Requirements and Specific Test Methods*, Standard IEC 61800-3, 2017.

[2] *Industrial Scientific and Medical Equipment-Radio-Frequency Disturbance Characteristics-Limits and Methods of Measurement*, CISPR, Geneva, Switzerland, 2015, vol. 11.

[3] D. Astigarraga, F. M. Ibanez, A. Galarza, J. M. Echeverria, I. Unanue, P. Baraldi, and E. Zio, "Analysis of the results of accelerated aging tests in insulated gate bipolar transistors," *IEEE Trans. Power Electron.*, vol. 31, no. 11, pp. 7953–7962, Nov. 2016.

[4] B. Wunsch, S. Skibin, V. Forsström, and I. Stevanovic, "EMC component modeling and system-level simulations of power converters: AC motor drives," *Energies*, vol. 14, no. 6, p. 1568, Mar. 2021.

[5] F. A. Kharanaq, A. Emadi, and B. Bilgin, "Modeling of conducted emissions for EMI analysis of power converters: State-of-the-art review," *IEEE Access*, vol. 8, pp. 189313–189325, 2020.

[6] H. Ott, *Electromagnetic Compatibility Engineering*. Hoboken, NJ, USA: Wiley, 2011.

[7] M. Feliziani and F. Maradei, "Full-wave analysis of shielded cable configurations by the FDTD method," *IEEE Trans. Electromagn. Magn.*, vol. 38, no. 2, pp. 761–764, Mar. 2002.

[8] H. Bagci, A. E. Yilmaz, J.-M. Jin, and E. Michielssen, "Fast and rigorous analysis of EMC/EMI phenomena on electrically large and complex cable-loaded structures," *IEEE Trans. Electromagn. Compat.*, vol. 49, no. 2, pp. 361–381, May 2007.

[9] Q. F. Liu, W. Y. Yin, M. Tang, P. G. Liu, J. F. Mao, and Q. H. Liu, "Time-domain investigation on cable-induced transient coupling into metallic enclosures," *IEEE Trans. Electromagn. Compat.*, vol. 51, no. 4, pp. 953–962, Nov. 2009.

[10] J. Wang, X. Han, K. Yang, Y. S. Xia, and W. Y. Yin, "Hybrid FDTD method for studying electromagnetic coupling effects of transmission line networks," *IEEE Trans. Electromagn. Compat.*, vol. 59, no. 5, pp. 1650–1653, Oct. 2017.

[11] A. Tatematsu, "A technique for representing lossy thin wires and coaxial cables for FDTD-based surge simulations," *IEEE Trans. Electromagn. Compat.*, vol. 60, no. 3, pp. 705–715, Jun. 2018.

[12] Y. Zhou, Y. Wang, and W. Wang, "A study on the propagation characteristics of partial discharge in cable joints based on the FDTD method," *IEEE Access*, vol. 8, pp. 130094–130103, 2020.

[13] F. M. Tesche, "Topological concepts for internal EMP interaction," *IEEE Trans. Electromagn. Compat.*, vol. EMC-20, no. 1, pp. 60–64, Feb. 1978.

[14] C. E. Baum, T. K. Liu, and F. M. Tesche, "On the analysis of general multiconductor transmission line networks," Kirtland AFB, Albuquerque, NM, USA, Interact. Note 350, 1978.

[15] C. E. Baum, "Electromagnetic topology for the analysis and design of complex electromagnetic system," in *Fast Electrical and Optical Measurements*, vol. 1. Leiden, The Netherlands: Martinus Nijhoff, 1986, pp. 467–547.

[16] C. E. Baum, "Generalization of the BLT equation," Kirtland AFB, Albuquerque, NM, USA, Interact. Note 511, Apr. 1995.

[17] F. M. Tesche and C. M. Butler, "On the addition of EM field propagation and coupling effects in the BLT equation," Kirtland AFB, Albuquerque, NM, USA, Interact. Note 588, Dec. 2003.

[18] F. M. Tesche, "Development and use of the BLT equation in the time domain as applied to a coaxial cable," *IEEE Trans. Electromagn. Compat.*, vol. 49, no. 1, pp. 3–11, Feb. 2007.

[19] F. M. Tesche, "On the analysis of a transmission line with nonlinear terminations using the time-dependent BLT equation," *IEEE Trans. Electromagn. Compat.*, vol. 49, no. 2, pp. 427–433, May 2007.

[20] G. Kron, "A method of solving very large physical systems in easy stages," *Proc. IRE*, vol. 42, no. 4, pp. 680–686, Apr. 1954.

[21] S. Leman, A. Reineix, F. Hoëppe, Y. Poiré, M. Mahmoudi, B. Démoulin, F. Üstüner, and V. P. Rodriguez, "KRON's method applied to the study of electromagnetic interference occurring in aerospace systems," in *Proc. ESA Workshop Aerosp. EMC*, Venice, Italy, 2012, pp. 1–6.

[22] S. Leman and F. Hoëppe, "Advanced spacecraft EM modelling based on geometric simplification process and multi-methods simulation," in *Proc. ESA Workshop Aerosp. EMC (Aerospace EMC)*, Valencia, Spain, May 2016, pp. 1–6.

[23] C. R. Paul, "A brief history of work in transmission lines for EMC applications," *IEEE Trans. Electromagn. Compat.*, vol. 49, no. 2, pp. 237–252, May 2007.

[24] C. R. Paul, *Analysis of Multiconductor Transmission Lines*, 2nd ed. New York, NY, USA: Wiley, 2008.

[25] C. R. Paul, *Transmission Lines in Digital and Analog Electronic Systems: Signal Integrity and Crosstalk*. Hoboken, NJ, USA: Wiley, 2010.

[26] C. L. Holloway, E. F. Kuester, A. E. Ruehli, and G. Antonini, "Partial and internal inductance: Two of clayton R. Paul's many passions," *IEEE Trans. Electromagn. Compat.*, vol. 55, no. 4, pp. 600–613, Aug. 2013.

[27] G. Antonini, A. Orlandi, and S. A. Pignari, "Review of clayton R. Paul studies on multiconductor transmission lines," *IEEE Trans. Electromagn. Compat.*, vol. 55, no. 4, pp. 639–647, Aug. 2013.

[28] N. S. Nahman and D. R. Halt, "Transient analysis of coaxial cables using the skin effect approximation," *IEEE Trans. Circuit Theory*, vol. CT-19, no. 5, pp. 443–451, Sep. 1972.

[29] A. Orlandi and C. R. Paul, "FDTD analysis of lossy, multiconductor transmission lines terminated in arbitrary loads," *IEEE Trans. Electromagn. Compat.*, vol. 38, no. 3, pp. 388–399, Aug. 1996.

[30] J. A. Roden, C. R. Paul, W. T. Smith, and S. D. Gedney, "Finite-difference, time-domain analysis of lossy transmission lines," *IEEE Trans. Electromagn. Compat.*, vol. 38, no. 1, pp. 15–23, Feb. 1996.

[31] G. Antonini, A. Orlandi, and C. R. Paul, "An improved method of modeling lossy transmission lines in finite-difference, time-domain analysis," in *Proc. IEEE Int. Symp. Electromagn. Compatability. Symp. Rec.*, Aug. 1999, pp. 435–439.

[32] N. Boulejfen, A. B. Kouki, and F. M. Ghannouchi, "Frequency- and time-domain analyses of nonuniform lossy coupled transmission lines with linear and nonlinear terminations," *IEEE Trans. Microw. Theory Techn.*, vol. 48, no. 3, pp. 367–379, Mar. 2000.

[33] S. Barmada, A. Musolino, and R. Rizzo, "Analysis of transmission lines with frequency-dependent parameters by wavelet-FFT method," *IEEE Trans. Magn.*, vol. 39, no. 3, pp. 1602–1605, May 2003.

[34] J. R. Marti and A. Tavighi, "Frequency-dependent multiconductor transmission line model with collocated voltage and current propagation," *IEEE Trans. Power Del.*, vol. 33, no. 1, pp. 71–81, Feb. 2018.

[35] Y. Huangfu, L. Di Rienzo, and S. Wang, "FDTD formulation based on high-order surface impedance boundary conditions for frequency-dependent lossy multi-conductor transmission lines," *IEEE Trans. Magn.*, vol. 56, no. 1, pp. 1–4, Jan. 2020.

[36] Y. Huangfu, L. Di Rienzo, and S. Wang, "FDTD formulation based on high-order surface impedance boundary conditions for lossy two-conductor transmission lines," *IEEE Trans. Electromagn. Compat.*, vol. 62, no. 1, pp. 194–203, Feb. 2020.

[37] B. Honarbakhsh and S. Asadi, "Analysis of multiconductor transmission lines using the CN-FDTD method," *IEEE Trans. Electromagn. Compat.*, vol. 62, no. 6, pp. 2823–2831, Dec. 2020.

[38] C. Paul and J. McKnight, "Prediction of crosstalk involving twisted pairs of wires—Part I: A transmission-line model for twisted-wire pairs," *IEEE Trans. Electromagn. Compat.*, vol. EMC-21, no. 2, pp. 92–105, May 1979.

[39] C. R. Paul, "A SPICE model for multiconductor transmission lines excited by an incident electromagnetic field," *IEEE Trans. Electromagn. Compat.*, vol. 36, no. 4, pp. 342–354, Nov. 1994.

[40] A. Shoory, M. Rubinstein, A. Rubinstein, C. Romero, N. Mora, and F. Rachidi, "Application of the cascaded transmission line theory of Paul and McKnight to the evaluation of NEXT and FEXT in twisted wire pair bundles," *IEEE Trans. Electromagn. Compat.*, vol. 55, no. 4, pp. 648–656, Aug. 2013.
[41] G. Spadacini, F. Grassi, and S. A. Pignari, "Field-to-wire coupling model for the common mode in random bundles of twisted-wire pairs," *IEEE Trans. Electromagn. Compat.*, vol. 57, no. 5, pp. 1246–1254, Oct. 2015.
[42] S. Belkhelfa, M. Lefouili, and K. E. K. Drissi, "Frequency domain analysis of EM crosstalk problem in a quad by the equivalent cable bundle method among twisted-wire pairs cable bundle," *IEEE Trans. Magn.*, vol. 51, no. 11, pp. 1–4, Nov. 2015.
[43] Y. Sun, J. Wang, W. Song, and R. Xue, "Frequency domain analysis of lossy and non-uniform twisted wire pair," *IEEE Access*, vol. 7, pp. 52640–52649, 2019.
[44] S. Wang, Z. Guo, T. Zhu, H. Feng, and S. Wang, "A new multi-conductor transmission line model of transformer winding for frequency response analysis considering the frequency-dependent property of the lamination core," *Energies*, vol. 11, no. 4, p. 826, Apr. 2018.
[45] F. Broydé and E. Clavelier, "A new method for the reduction of crosstalk and echo in multiconductor interconnections," *IEEE Trans. Circuits Syst. I, Reg. Papers*, vol. 52, no. 2, pp. 405–416, Feb. 2005.
[46] J. Seo, M. Choi, and B. Kim, "An approximate closed-form transfer function model for multiconductor transmission lines," *IEEE Trans. Circuits Syst. II, Exp. Briefs*, vol. 65, no. 9, pp. 1199–1203, Sep. 2018.
[47] J. A. B. Faria, "The transfer matrix method: Analysis of nonuniform multiport systems," *IEEE Access*, vol. 8, pp. 23605–23662, 2020.
[48] Y. Huangfu, L. Di Rienzo, and S. Wang, "Frequency-dependent multiconductor transmission line model for shielded power cables considering geometrical dissymmetry," *IEEE Trans. Magn.*, vol. 54, no. 3, pp. 1–4, Mar. 2018.
[49] J. E. Bracken, "Mutual resistance in spicelink," Ansoft Corp., Pittsburgh, PA, USA, Sep. 2000.
[50] C. R. Paul, "What do we mean by 'inductance'? Part II: Partial inductance," *IEEE EMC Soc. Mag.*, pp. 72–79, 2008.
[51] C. R. Paul, *Inductance: Loop and Partial*. Hoboken, NJ, USA: Wiley, 2010.
[52] H. T. Steenstra and A. P. J. V. Deursen, "Reduction of conducted interference by steel armor in buried cables: Measurements and modeling," *IEEE Trans. Electromagn. Compat.*, vol. 50, no. 3, pp. 678–686, Aug. 2008.
[53] Y. Liu, S. A. Sebo, R. Caldecott, D. G. Kasten, and S. E. Wright, "Modeling of converter transformers using frequency domain terminal impedance measurements," *IEEE Trans. Power Del.*, vol. 8, no. 1, pp. 66–72, Jan. 1993.
[54] *Q3D Extractor Help, Release 2020 R1*. Accessed: Jan. 2020. [Online]. Available: https://www.ansys.com/products/electronics/ansys-q3d-extractor
[55] C. Marlier, A. Videt, and N. Idir, "NIF-based frequency-domain modeling method of three-wire shielded energy cables for EMC simulation," *IEEE Trans. Electromagn. Compat.*, vol. 57, no. 1, pp. 145–155, Feb. 2015.
[56] B. Gustavsen and A. Semlyen, "Rational approximation of frequency domain responses by vector fitting," *IEEE Trans. Power Del.*, vol. 14, no. 3, pp. 1052–1061, Jul. 1999.
[57] B. Gustavsen, "Improving the pole relocating properties of vector fitting," *IEEE Trans. Power Del.*, vol. 21, no. 3, pp. 1587–1592, Jul. 2006.
[58] D. Deschrijver, M. Mrozowski, T. Dhaene, and D. D. Zutter, "Macromodeling of multiport systems using a fast implementation of the vector fitting method," *IEEE Microw. Wireless Compon. Lett.*, vol. 18, no. 6, pp. 383–385, Jun. 2008.
[59] B. Gustavsen, "Fast passivity enforcement for pole-residue models by perturbation of residue matrix eigenvalues," *IEEE Trans. Power Del.*, vol. 23, no. 4, pp. 2278–2285, Oct. 2008.
[60] A. Semlyen and B. Gustavsen, "A half-size singularity test matrix for fast and reliable passivity assessment of rational models," *IEEE Trans. Power Del.*, vol. 24, no. 1, pp. 345–351, Jan. 2009.
[61] G. Antonini, "SPICE equivalent circuits of frequency-domain responses," *IEEE Trans. Electromagn. Compat.*, vol. 45, no. 3, pp. 502–512, Aug. 2003.

YOUPENG HUANGFU (Member, IEEE) received the B.Sc. degree in electrical engineering from Jilin University, Changchun, China, in 2012, and the Ph.D. degree in electrical engineering from the Politecnico di Milano, Milan, Italy, and Xi'an Jiaotong University, Xi'an, China, in 2019. He is currently a Research Associate with the Dipartimento di Elettronica, Informazione e Bioingegneria, Politecnico di Milano. His current research interests include the finite difference time domain method and macromodeling methods for time-domain analysis of lossy multiconductor transmission lines, electromagnetic compatibility, and arc fault detection approaches for aerospace electrical systems.

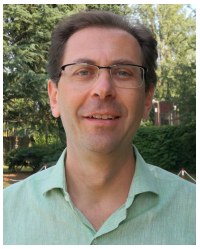

LUCA DI RIENZO (Senior Member, IEEE) received the Laurea (M.Sc.) *(cum laude)* and Ph.D. degrees in electrical engineering from the Politecnico di Milano, in 1996 and 2001, respectively, and the B.S. degree *(cum laude)* in mathematics from the Università Statale di Milano, in 2020. He is currently an Associate Professor with the Dipartimento di Elettronica, Informazione e Bioingegneria, Politecnico di Milano. His current research interests include the field of computational electromagnetics, including magnetic inverse problems, integral equation methods, surface impedance boundary conditions, and uncertainty quantification. He is an Associate Editor-in-Chief of *The Applied Computational Electromagnetics Society Journal* and an Editorial Board Member of *COMPEL-The International Journal for Computation and Mathematics in Electrical and Electronic Engineering* and *Sensing and Imaging*.

SHULI YIN received the B.Sc. degree in survey and control technology and instrument from Jilin University, Changchun, China, in 2012. She is currently pursuing the dual Ph.D. degree in electrical engineering with Xi'an Jiaotong University, Xi'an, China, and the Politecnico di Milano, Milan, Italy. Her current research interests include eddy currents, electromagnetic field theory and its applications, and analytical and numerical methods in solving electromagnetic problems.